
MOX–Report No. 33/2011

# Hierarchical a posteriori error estimators for the mimetic discretization of elliptic problems

Antonietti, P.F.; Beirao da Veiga, L.; Lovadina, C.; Verani, M.

MOX, Dipartimento di Matematica "F. Brioschi"
Politecnico di Milano, Via Bonardi 9 - 20133 Milano (Italy)

mox@mate.polimi.it http://mox.polimi.it

# Hierarchical a posteriori error estimators for the mimetic discretization of elliptic problems

Paola F. Antonietti[a], Lourenco Beirão da Veiga[b], Carlo Lovadina[c] and Marco Verani[d]

July 25, 2011

[a] MOX, Dipartimento di Matematica, Politecnico di Milano
Piazza Leonardo da Vinci 32, I-20133 Milano, Italy
E-mail: paola.antonietti@polimi.it

[b] Dipartimento di Matematica, Università di Milano
Via Saldini 50, I-20133 Milano, Italy
E-mail: lourenco.beirao@unimi.it

[c] Dipartimento di Matematica, Università di Pavia
Via Ferrata 1, I-27100 pavia, Italy
E-mail: carlo.lovadina@unipv.it

[d] MOX, Dipartimento di Matematica, Politecnico di Milano
Piazza Leonardo da Vinci 32, I-20133 Milano, Italy
E-mail: marco.verani@polimi.it

**Abstract**

We present an a posteriori error estimate of hierarchical type for the mimetic discretization of elliptic problems. Under a saturation assumption, the global reliability and efficiency of the proposed a posteriori estimator has been proved. Several numerical experiments assess the actual performance of the local error indicators in driving adaptive mesh refinement algorithms based on different marking strategies. Finally, we test an heuristic variant of the proposed error estimator which drastically reduces the overall computational cost of the adaptive procedures.

## 1 Introduction

A posteriori error indicators are key ingredients to design efficient adaptive algorithms for the numerical solution of partial differential equations. In recent years, the a posteriori error analysis of finite element and finite volume methods has been the object of an intensive research activity (see e.g. [30, 1, 3] and the references therein), while recently, the convergence and optimality properties of adaptive finite element (AFEM) methods have been addressed in several works (see e.g. [28] and references therein). More recently, thanks to the flexibility of the mesh and the possibility to mimic the intrinsic properties of the differential problem under study, the mimetic finite difference (MFD) method has been successfully applied to a large class of differential problems, a very partial list including [15, 16, 9, 7, 2, 17, 18, 11, 22, 24, 25] and [23, 26, 29, 31, 27] for some example of other non-standard related methods. The flexibility of MFD methods makes them very well suited for the application of adaptive strategies

for error control. Although the a priori analysis of this family of methods has been intensively addressed for second order elliptic problems [15, 14, 8], nevertheless the corresponding a posteriori analysis has not reached a comparable level of maturity (see e.g. [6, 10] for MFD method in its mixed formulation). In this paper, we develop and analyze new a posteriori error estimator (of hierachical type) for MFD methods in primal formulation applied to linear elliptic problems. To our knowledge this represents the first result along this direction.

The paper is organized as follows. In Section 2 we present the problem, while in Section 3 we address its mimetic discretization. In Section 4 we present our a posteriori error estimator and we prove global reliability and efficiency, under a saturation assumption. We also propose an alternative heuristic error estimator, which drastically reduces the overall computational cost of the adaptive algorithm. Finally, in Section 5 several numerical results assess the effectiveness of our a posteriori error estimator and of its heuristic variant when employed in driving adaptive algorithms.

## 2 The continuous problem

Throughout the paper we will use standard notations for Sobolev spaces, norms and seminorms. Let $\Omega$ be an open, bounded domain of $\mathbb{R}^2$, with polygonal boundary $\Gamma := \partial\Omega$. Let us introduce the bilinear form $a(u,v) : H^1(\Omega) \times H^1(\Omega) \longrightarrow \mathbb{R}$ defined by

$$a(u,v) := \int_\Omega \nabla u \cdot \nabla v \, \mathrm{d}x,$$

and the linear functional $f(v) : L^2(\Omega) \longrightarrow \mathbb{R}$ with

$$f(v) := \int_\Omega f \; v \, \mathrm{d}x,$$

where we assume $f \in L^2(\Omega)$.

Then, assuming homogeneous Dirichlet boundary conditions, the diffusion problem in variational form reads:

$$\begin{cases} \text{Find } u \in H^1_0(\Omega) \text{ such that} \\ a(u,v) = f(v) \qquad \forall v \in H^1_0(\Omega). \end{cases} \tag{1}$$

It is well known [13] that the above problem admits a unique solution.

## 3 A mimetic discretization

We now briefly review the mimetic discretization method for problem (1) presented in [14] and extended to arbitrary polynomial order in [8].

### 3.1 Mesh notation and assumptions

Let $\Omega_h \subset \Omega$ be a polygonal approximation of $\Omega$, in such a way that all vertexes of $\Omega_h$ which are on the boundary of $\Omega_h$ are also on the boundary of $\Omega$. The polygonal domain $\Omega_h$ represents the computational domain for the method.

With a little abuse of notation, we also indicate with $\Omega_h$ a partition of the above introduced computational domain into polygons $E$. We assume that this partition is conformal, *i.e.*, intersection of two different elements $E_1$ and $E_2$ is either a few mesh points, or a few mesh edges (two adjacent elements may share more than one edge) or empty. We allow $\Omega_h$ to contain non-convex elements. Note moreover that, differently from conforming finite elements meshes, T-junctions are now allowed in the mesh; indeed, these are included in the above conditions simply by splitting single edges into two new (aligned) edges. For each polygon $E$, $|E|$ denotes its area, $h_E$ denotes its diameter and

$$h := \max_{E \in \Omega_h} h_E.$$

We denote the set of mesh vertexes and edges by $\mathcal{N}_h$ and $\mathcal{E}_h$, the set of internal vertexes and edges by $\mathcal{N}_h^i$ and $\mathcal{E}_h^i$, the set of boundary vertexes and edges by $\mathcal{N}_h^\partial$ and $\mathcal{E}_h^\partial$. We denote a generic mesh vertex by $\mathsf{v}$, a generic edge by $e$ and its length both by $h_e$ and $|e|$. The vertexes and edges of a particular element $E$ are always considered as elements of $\partial E$, the notation made clear by the adopted symbol; for instance, $\{\mathsf{v}\}_{\mathsf{v} \in \partial E}$ indicates the set of vertexes of $E$, while $\{e\}_{e \in \partial E}$ indicates the set of edges.

A fixed orientation is also set for the mesh $\Omega_h$, which is reflected by a unit normal vector $\mathbf{n}_e$, $e \in \mathcal{E}_h$, fixed once for all. For every polygon $E$ and edge $e \in \mathcal{E}_h^E$, we define a unit normal vector $\mathbf{n}_E^e$ that points outside of $E$.

The mesh is assumed to satisfy the following shape regularity properties, which have already been used in [14].

There exist

- an integer number $N_s$ independent of $h$;
- a real positive number $\rho$ independent of $h$;
- a *compatible* sub-decomposition $\mathcal{T}_h$ of every $\Omega_h$ into shape-regular triangles,

such that

(H1) any polygon $E \in \Omega_h$ admits a decomposition $\mathcal{T}_h|_E$ formed by less than $N_s$ triangles;

(H2) any triangle $T \in \mathcal{T}_h$ is shape-regular in the sense that the ratio between the radius $r$ of the inscribed ball and the diameter $h_T$ of $T$ is bounded from below by $\rho$:

$$0 < \rho \leq \frac{r}{h_T}.$$

From (H1), (H2) there can be easily derived the following useful properties we list below.

(M1) The number of vertexes and edges of every polygon $E$ of $\Omega_h$ are *uniformly* bounded from above by two integer numbers $N_\mathsf{v}$ and $N_e$, which only depend on $N_s$.

(M2) There exists a real positive number $\sigma_s$, which only depends on $N_s$ and $\rho$, such that

$$h_e \geq \sigma_s h_E \qquad \text{and} \qquad |E| \geq \sigma_s h_E^2,$$

for every polygon $E$ of every decomposition $\Omega_h$, for every edge $e$ of $E$.

(M3) There exists a constant $C_a$, only dependent on $\rho$ and $N_s$, such that for every polygon $E$, for every edge $e$ of $E$ and for every function $\psi \in H^1(E)$, the following *trace inequality* holds:

$$\|\psi\|^2_{L^2(e)} \leq C_a\Big(h_E^{-1}\|\psi\|^2_{L^2(E)} + h_E\,|\psi|^2_{H^1(E)}\Big). \tag{2}$$

(M4) There exists a constant $C_{app}$, which is independent of $h$, such that the following holds. For every $E$ and for every function $\psi \in H^m(E)$, $m \in \mathbb{N}$, there exists a polynomial $\psi_k$ of degree $k$ living on $E$ such that

$$|\psi - \psi_k|_{H^l(E)} \leq C_{app} h_E^{m-l}\,|\psi|_{H^m(E)}$$

for all integers $0 \leq l \leq m \leq k+1$.

Note that (M4) follows, for instance, from the extended Bramble-Hilbert lemma on non star-shaped domains of [21, 13]; an explicit proof can be found in [2].

### 3.2 Degrees of freedom and interpolation operators

To describe the discretization of problem (1), we start introducing the discrete approximation space $V_h$ which is defined as follows: a vector $v_h \in V_h$ consists of a collection of degrees of freedom

$$v_h := \{v_h(\mathsf{v})\}_{\mathsf{v}\in\mathcal{N}_h},$$

one per mesh vertex, *e.g.* to every vertex $\mathsf{v} \in \mathcal{N}_h^i$, we associate a real number $v_h(\mathsf{v})$. The scalar $v_h(\mathsf{v})$ represents the nodal value of the underlying discrete scalar field of displacement. Moreover, for all nodes of the mesh which lay on the boundary we will assume

$$v_h(\mathsf{v}) = 0 \quad \forall v_h \in V_h, \forall \mathsf{v} \in \mathcal{N}_h^\partial.$$

Therefore, the number of unknowns of $V_h$ is equal to the number of internal vertexes of the mesh.

We now introduce an interpolation operator $I$ into the discrete space $V_h$: for every function $v \in \mathcal{C}^0(\bar{\Omega}) \cap H^1(\Omega)$, we define $v_I \in V_h$ by

$$v_I(\mathsf{v}) := v(\mathsf{v}) \quad \forall \mathsf{v} \in \mathcal{N}_h.$$

Moreover, we analogously define the local interpolation operator from $\mathcal{C}^0(\bar{E}) \cap H^1(E)$ into $V_h|_E$ given by

$$v_I(\mathsf{v}) := v(\mathsf{v}) \quad \forall \mathsf{v} \in \partial E. \tag{3}$$

### 3.3 Discrete norms and bilinear forms

For each polygon $E \in \Omega_h$ we introduce the seminorm:

$$\|v_h\|^2_{1,h,E} := \left(|E| \sum_{e\in\partial E} \left[\frac{1}{|e|}\left(v_h(\mathsf{v}_2) - v_h(\mathsf{v}_1)\right)\right]^2\right) \simeq \sum_{e\in\partial E} \big(v_h(\mathsf{v}_2) - v_h(\mathsf{v}_1)\big)^2, \tag{4}$$

where $\mathsf{v}_1$ and $\mathsf{v}_2$ denote the two vertexes of $e$, and the symbol $\simeq$ indicates equivalence up to a uniform constant (c.f. assumption (M2)).

We endow the space $V_h$ with the following discrete norm

$$\|v_h\|_{1,h}^2 := \sum_{E\in\Omega_h} \|v_h\|_{1,h,E}^2 \simeq \sum_{E\in\Omega_h}\sum_{e\in\partial E} \big(v_h(\mathsf{v}_2) - v_h(\mathsf{v}_1)\big)^2. \tag{5}$$

Due to the homogeneous Dirichlet boundary conditions, the quantity $\|\cdot\|_{1,h}$ is a norm on $V_h$. We remark that $\|\cdot\|_{1,h}$ is a sort of discrete $H^1(\Omega)$ norm. Indeed, the differences $\frac{1}{|e|}(v_h(\mathsf{v}_2) - v_h(\mathsf{v}_1))$ represent (tangential) gradients on edges and the scalings with respect to $h_E$ and $h_e$ are the correct ones to mimic an $H^1(E)$ local seminorm.

We denote by $a_h(\cdot,\cdot) : V_h \times V_h \to \mathbb{R}$ the discretization of the bilinear form $a(\cdot,\cdot)$, defined as follows:

$$a_h(v_h, w_h) := \sum_{E\in\Omega_h} a_h^E(v_h, w_h) \quad \forall v_h, w_h \in V_h, \tag{6}$$

where $a_h^E(\cdot,\cdot)$ is a symmetric bilinear form on each element $E$. The local forms mimic

$$a_h^E(v_h, w_h) \sim \int_E \nabla\widetilde{v}_h \cdot \nabla\widetilde{w}_h \,\mathrm{d}x,$$

where, roughly speaking, $\widetilde{v}_h, \widetilde{w}_h$ denote regular functions living on $E$ which "extend the data" $v_h, w_h$ inside the element.

We introduce two fundamental assumptions for the local bilinear form $a_h^E(\cdot,\cdot)$. The first one represents the coercivity with respect to the local seminorm as well as and the correct scaling with respect to the element size.

(S1) there exist two positive constants $c_1$ and $c_2$ independent of $h$ such that, for every $u_h, v_h \in V_h$ and each $E \in \Omega_h$, we have

$$c_1\|v_h\|_{1,h,E}^2 \le a_h^E(v_h, v_h) \le c_2\|v_h\|_{1,h,E}^2. \tag{7}$$

In order to introduce the second assumption, we observe beforehand that, using an integration by parts,

$$\int_E \nabla v \cdot \nabla q \,\mathrm{d}x = -\int_E (\Delta q) v \,\mathrm{d}x + \sum_{e\in\partial E}\int_e (\nabla q \cdot \mathbf{n}_E^e) v \,\mathrm{d}s = \sum_{e\in\partial E} \nabla q \cdot \mathbf{n}_E^e \int_e v \,\mathrm{d}s \tag{8}$$

for all $E \in \Omega_h$, for all $v \in [H^1(E)]^2$ and for all linear functions $q$. By substituting the integral in the last term of (8) with a trapezium integration rule gives our second condition

(S2) For every element $E$, every linear vector function $q$ on $E$, and every $v_h \in V_h$, it holds

$$a_h^E(v_h, q) = \sum_{e\in\partial E} (\nabla q \cdot \mathbf{n}_E^e)\frac{|e|}{2}\big(v_h(\mathsf{v}_1) + v_h(\mathsf{v}_2)\big), \tag{9}$$

where $\mathsf{v}_1$ and $\mathsf{v}_2$ are the two vertexes of $e \in \mathbf{n}_E^e$.

The meaning of the above consistency condition (S2) is therefore that the discrete bilinear form satisfies integration by parts when tested with linear functions.

**Remark 3.1** *The scalar product and the bilinear form shown in this section can be easily built element by element in a simple algebraic way. See for instance [14, 2].*

### 3.4 The discrete method

Finally, we are able to define the proposed mimetic discrete method for the diffusion problem (1). Let the loading term

$$(f, v_h)_h := \sum_{E\in\Omega_h} \bar{f}|_E \sum_{i=1}^{k_E} v_h(\mathsf{v}_i)\,\omega_E^i, \tag{10}$$

where $\mathsf{v}_1, \ldots, \mathsf{v}_{k_E}$ are the vertexes of $E$, $\bar{f}|_E := \frac{1}{|E|}\int_E f\,\mathrm{d}x$, and $\omega_E^1, \ldots, \omega_E^{k_E}$ are positive weights such that $\sum_{i=1}^{k_E} \omega_E^i = |E|$. The loading term (10) is clearly an integral approximation

$$(f, v_h)_h \sim \int_\Omega f\tilde{v}_h\,\mathrm{d}x,$$

which is exact for constant functions.

Then, the mimetic discretization of problem (1) reads:

$$\begin{cases} \text{Find } u_h \in V_h \text{ such that} \\ a_h(u_h, v_h) = (f, v_h)_h \qquad \forall v_h \in V_h. \end{cases} \tag{11}$$

Due to property (S1) it is straightforward to check that the bilinear form $a_h(\cdot,\cdot)$ is coercive on $V_h$. As a consequence, existence and uniqueness of the solution to the discrete problem (11) trivially follows.

## 4 A posteriori error estimate

In this section we perform a posteriori error analysis of the mimetic finite difference method described in Section 3. The a posteriori error indicators that we propose and analyze belong to the class of non-residual type, in particular of hierarchical type (see e.g. [4, 1] and the references therein for the finite element framework).

In the following, we state some preliminary key results concerning mesh refinement.

### 4.1 Mesh refinement and related results

Given a mesh $\Omega_h$ we can build a uniformly refined mesh $\widehat{\Omega}_h$ as follows. We start assuming that

(H3) all polygons $E \in \Omega_h$ are convex.

Then, we introduce the point $\mathbf{x}_E \in E$

$$\mathbf{x}_E := \frac{1}{N}\sum_{\mathsf{v}\in\partial E} \mathbf{x}(\mathsf{v})\ , \tag{12}$$

where $N$ is the number of vertexes in $\partial E$ and $\mathbf{x}(\mathsf{v})$ is the position vector of node $\mathsf{v} \in \mathcal{N}$.

**Remark 4.1** *We remark that assumption (H3) is made essentially for the sake of exposition simplicity. What follows can be adapted to cover more general cases such as, for instance, elements which are star shaped with respect to a ball. In particular,* (12) *has to be modified to define an interior point, and* (15) *has to be changed, for* $\mathsf{v} = \mathbf{x}_E$*, in such a way that the operator preserves the linear functions.*

The uniformly refined mesh $\widehat{\Omega}_h$ is built by subdividing each element $E$ of $\Omega_h$ in the following way: each midpoint $\mathsf{m} = \mathsf{m}(e)$ of each edge $e \in \partial E$ is connected with the point $\mathbf{x}_E$. This determines a subdivision of $E$ into sub-elements which are collected for all $E \in \Omega_h$ to form the new mesh $\widehat{\Omega}_h$ (see Figure 1). In the following, we will indicate all geometrical objects of the finer grid $\widehat{\Omega}_h$ with a hat symbol, the meaning being the same as in the original mesh. For instance, we will indicate with $\widehat{E}$ a generic element of $\widehat{\Omega}_h$, and with $\widehat{\mathcal{N}}$ the set of all its vertexes. Note that

$$\widehat{\mathcal{N}} = \mathcal{N} \cup \{\mathsf{m}(e)\}_{e\in\mathcal{E}} \cup \{\mathbf{x}_E\}_{E\in\Omega_h},$$

i.e. the edge midpoints $\mathsf{m}(e)$ and the points $\mathbf{x}_E$ become additional vertexes in the new mesh $\widehat{\Omega}_h$. In addition, $\hat{h}$ will denote the mesh-size of the finer mesh $\widehat{\Omega}_h$. Following the construction

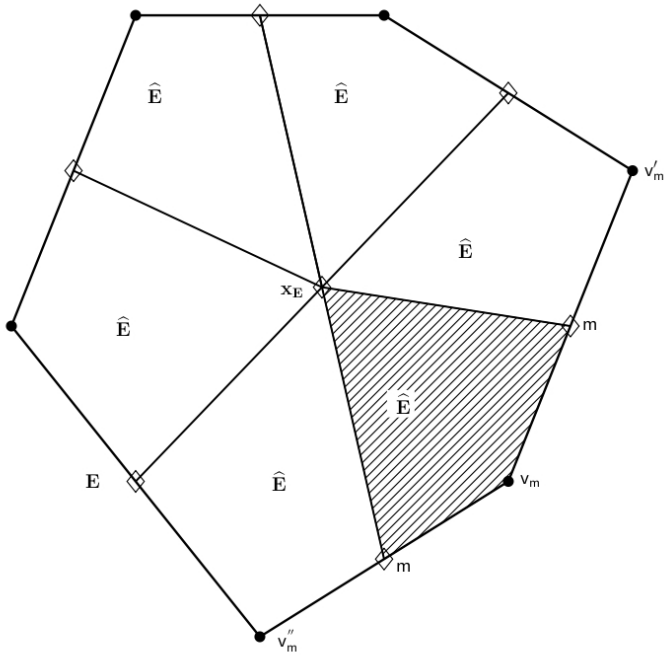


Figure 1: Refinement strategy: coarse element $E$ and sub-elements $\widehat{E}$. Circles denote the coarse vertexes, while diamonds refer to additional vertexes in the finer mesh.

given in section 3, we can introduce a finer discrete space $\widehat{V}_h$ associated to the mesh $\widehat{\Omega}_h$, a bilinear form $\widehat{a}_h(\cdot,\cdot) : \widehat{V}_h \times \widehat{V}_h \to \mathbb{R}$ and a suitable loading term, so that the finer version of

the coarse discrete problem (11) reads as follows

$$\begin{cases} \text{Find } \widehat{u}_h \in \widehat{V}_h \text{ such that} \\ \widehat{a}_h(\widehat{u}_h, v_h) = (f, v_h)_{\widehat{h}} \qquad \forall v_h \in \widehat{V}_h. \end{cases} \tag{13}$$

We now introduce two operators that maps the finer space into the coarser one and viceversa. Let $\Pi : \widehat{V}_h \to V_h$ be defined by

$$\big(\Pi(v_h)\big)(\mathsf{v}) = v_h(\mathsf{v}) \quad \forall \mathsf{v} \in \mathcal{N},\ \forall v_h \in \widehat{V}_h. \tag{14}$$

Given any midpoint $\mathsf{m} = \mathsf{m}(e)$, $e \in \mathcal{E}_h$, we indicate with $\mathsf{v}_\mathsf{m}$ and with $\mathsf{v}'_\mathsf{m}$ the two vertexes which are endpoints to the edge $e$. We then define $\Pi^\dagger : V_h \to \widehat{V}_h$ by

$$\big(\Pi^\dagger(v_h)\big)(\mathsf{v}) = \begin{cases} v_h(\mathsf{v}) & \forall \mathsf{v} \in \mathcal{N} \\ \dfrac{1}{2}\big(v_h(\mathsf{v}_\mathsf{m}) + v_h(\mathsf{v}'_\mathsf{m})\big) & \text{if } \mathsf{v} = \mathsf{m}(e),\ e \in \mathcal{E} \\ \dfrac{1}{N}\displaystyle\sum_{\mathsf{v} \in \partial E} v_h(\mathsf{v}) & \text{if } \mathsf{v} = \mathbf{x}_E,\ E \in \Omega_h, \end{cases} \tag{15}$$

for all $v_h \in V_h$. The operator $\Pi^\dagger$ embeds the coarse space $V_h$ into the finer space $\widehat{V}_h$ by averaging the coarse vertex values. We denote by $\widehat{V}_h^c$ the subspace of $\widehat{V}_h$ given by the image of $\Pi^\dagger$ and we refer to it as to the embedded coarse space. Finally, we introduce the fluctuation space

$$\widehat{V}_h^f = \{v_h \in \widehat{V}_h \mid v_h(\mathsf{v}) = 0\ \forall \mathsf{v} \in \mathcal{N}\}.$$

It is immediate to check that

$$\widehat{V}_h = \widehat{V}_h^c \oplus \widehat{V}_h^f.$$

Let $\|\cdot\|_{1,\widehat{h}}$ and $\|\cdot\|_{1,\widehat{h},\widehat{E}}$, $\widehat{E} \in \widehat{V}_h$, denote the global and local norms of the finer space $\widehat{V}_h$ (cfr. (5)). Accordingly, we indicate with $\|\cdot\|_{1,\widehat{h},E}$ the norm of the fine space restricted to the coarse element $E \in \Omega_h$

$$\|v_h\|^2_{1,\widehat{h},E} = \sum_{\widehat{E} \in E} \|v_h\|^2_{1,\widehat{h},\widehat{E}} \quad \forall v_h \in \widehat{V}_h.$$

The following result states a minimum angle condition among the two spaces $\widehat{V}_h^c$ and $\widehat{V}_h^f$.

**Lemma 4.1** *There exists a positive constant $C_m$ independent of $h$ such that for all $E \in \Omega_h$*

$$\|v_h^c\|_{1,\widehat{h},E} + \|v_h^f\|_{1,\widehat{h},E} \le C_m \|v_h^c + v_h^f\|_{1,\widehat{h},E} \tag{16}$$

*for all $v_h^c \in \widehat{V}_h^c$ and $v_h^f \in \widehat{V}_h^f$.*

*Proof.* To prove (16) it is sufficient to show

$$\|v_h^c\|_{1,\widehat{h},E} \le C \|v_h^c + v_h^f\|_{1,\widehat{h},E} \tag{17}$$

for all $v_h^c \in \widehat{V}_h^c$ and $v_h^f \in \widehat{V}_h^f$, since the other bound:

$$\|v_h^f\|_{1,\widehat{h},E} \le C \|v_h^c + v_h^f\|_{1,\widehat{h},E}$$

immediately follows from (17) using the triangle inequality. Furthermore, since $\Pi^\dagger(\Pi(v_h^c + v_h^f)) = v_h^c$ for all $v_h^c \in \widehat{V}_h^c$ and $v_h^f \in \widehat{V}_h^f$, bound (17) will hold true if we show the following estimate:

$$\|\Pi^\dagger(\Pi(v_h))\|_{1,\widehat{h},E} \leq C \|v_h\|_{1,\widehat{h},E} \quad \forall v_h \in \widehat{V}_h. \tag{18}$$

To shorten the notation, we set $w_h = \Pi^\dagger(\Pi(v_h))$. Using the definition of the norm, we get

$$\begin{aligned} \|w_h\|_{1,\widehat{h},E}^2 = &\sum_{\mathsf{m}\in\partial E} \big(w_h(\mathsf{v}_\mathsf{m}) - w_h(\mathsf{m})\big)^2 + \sum_{\mathsf{m}\in\partial E} \big(w_h(\mathsf{v}'_\mathsf{m}) - w_h(\mathsf{m})\big)^2 \\ &+ \sum_{\mathsf{m}\in\partial E} \big(w_h(\mathsf{m}) - w_h(\mathbf{x}_E)\big)^2, \end{aligned} \tag{19}$$

where we recall that $\mathsf{m}$ and $\mathsf{m}'$ denote the endpoints of the edge whose mid-point is $\mathsf{m}$, and $\mathbf{x}_E$ is defined by (12). Since the first and second term on the right-hand side of (19) can be treated in a similar way, we work out the details only of the first one. Using definitions (14) and (15) gives

$$\begin{aligned} \sum_{\mathsf{m}\in\partial E} \big(w_h(\mathsf{v}_\mathsf{m}) - w_h(\mathsf{m})\big)^2 &= \sum_{\mathsf{m}\in\partial E} \frac{1}{4}\big(w_h(\mathsf{v}_\mathsf{m}) - w_h(\mathsf{v}'_\mathsf{m})\big)^2 \\ &= \sum_{\mathsf{m}\in\partial E} \frac{1}{4}\Big[\big(\Pi(v_h)\big)(\mathsf{v}_\mathsf{m}) - \big(\Pi(v_h)\big)(\mathsf{v}'_\mathsf{m})\Big]^2 \\ &\leq C \|\Pi(v_h)\|_{1,h,E}^2. \end{aligned} \tag{20}$$

From definition (15) and the triangle inequality we get

$$|w_h(\mathsf{m}) - w_h(\mathbf{x}_E)| \leq \frac{1}{2}\Big(|w_h(\mathsf{v}_\mathsf{m}) - w_h(\mathbf{x}_E)| + |w_h(\mathsf{v}'_\mathsf{m}) - w_h(\mathbf{x}_E)|\Big),$$

and thus

$$\sum_{\mathsf{m}\in\partial E} \big(w_h(\mathsf{m}) - w_h(\mathbf{x}_E)\big)^2 \leq C \sum_{\mathsf{v}\in\partial E} \big(w_h(\mathsf{v}) - w_h(\mathbf{x}_E)\big)^2.$$

Using again definitions (14) and (15), writing $w_h(\mathsf{v}) = \frac{1}{N}\sum_{\mathsf{v}'\in\partial E} w_h(\mathsf{v}')$ and employing some simple algebra there follows

$$\begin{aligned} \sum_{\mathsf{v}\in\partial E} \big(w_h(\mathsf{v}) - w_h(\mathbf{x}_E)\big)^2 &\leq C \sum_{\mathsf{v}\in\partial E}\sum_{\mathsf{v}'\in\partial E} N^{-2}\big(w_h(\mathsf{v}) - w_h(\mathsf{v}')\big)^2 \\ &= C \sum_{\mathsf{v}\in\partial E}\sum_{\mathsf{v}'\in\partial E} N^{-2}\Big[\big(\Pi(v_h)\big)(\mathsf{v}) - \big(\Pi(v_h)\big)(\mathsf{v}')\Big]^2 \\ &\leq C \|\Pi(v_h)\|_{1,h,E}^2. \end{aligned} \tag{21}$$

Combining (19) with the above bounds yields

$$\|\Pi^\dagger(\Pi(v_h))\|_{1,\widehat{h},E}^2 \leq C \|\Pi(v_h)\|_{1,h,E}^2 \quad \forall v_h \in \widehat{V}_h. \tag{22}$$

Since the triangle inequality applied edge by edge easily give

$$\|\Pi(v_h)\|_{1,h,E}^2 \leq C \|v_h\|_{1,\widehat{h},E}^2, \tag{23}$$

bound (22) leads to (18), and thus the lemma is proved.
□

Note that, as a byproduct of the above proof, we obtained also the stronger bound (22), which gives the following simple lemma.

**Lemma 4.2** *There exist positive constants $C, C'$ such that for all $E \in \Omega_h$*

$$C\|v_h\|_{1,h,E} \leq \|\Pi^\dagger(v_h)\|_{1,\widehat{h},E} \leq C'\|v_h\|_{1,h,E} \quad \forall v_h \in V_h. \tag{24}$$

*Proof.* The first bound above follows immediately from the definition of the involved norms and a triangle inequality edge by edge. For the second bound we observe that $\Pi(\Pi^\dagger(v_h)) = v_h$ for all $v_h \in V_h$. Therefore, applying (22) we get

$$\|\Pi^\dagger(v_h)\|_{1,\widehat{h},E} = \|\Pi^\dagger(\Pi(\Pi^\dagger(v_h)))\|_{1,\widehat{h},E} \leq C'\|\Pi(\Pi^\dagger(v_h))\|_{1,h,E} = C'\|v_h\|_{1,h,E}.$$

□

## 4.2 A fully consistent coarse problem

In this section we present a convenient choice for the coarse bilinear form $a_h$ which allows some simplifications in the following a posteriori error analysis (see Corollary 4.1). However, the generality of our analysis will not be affected by such a particular choice.

As mentioned before, let $\widehat{a}_h(\cdot,\cdot)$ be any discrete bilinear form built on the space $\widehat{V}_h$ following the construction of Section 3.3. In other words, we assume that the bilinear form $\widehat{a}_h(\cdot,\cdot)$ is the sum of local forms $\widehat{a}_h^{\widehat{E}}(\cdot,\cdot)$, $\widehat{E} \in \widehat{\Omega}_h$, that satisfy ($\widehat{\mathsf{S1}}$) and ($\widehat{\mathsf{S2}}$) (the identic counterparts of (S1) and (S2) for the fine space and mesh).

Then, for all $E \in \Omega_h$, we can define a bilinear form $a_h^E(\cdot,\cdot)$ on the coarse space $V_h$ as follows

$$a_h^E(v_h, w_h) := \sum_{\widehat{E}\in E} \widehat{a}_h^{\widehat{E}}(\Pi^\dagger(v_h), \Pi^\dagger(w_h)) \quad \forall v_h, w_h \in V_h\ . \tag{25}$$

To guarantee the well-posedeness of the coarse problem (11), we need to show that (25) satisfies both (S1) and (S2); this will be addressed in the following.

**Lemma 4.3** *The bilinear form* (25) *satisfies (S1) and (S2).*

*Proof.* The proof of (S1) is immediate. First recalling definition (25), then using ($\widehat{\mathsf{S1}}$) and finally applying Lemma 4.2, yields for all $E \in \Omega_h$

$$\begin{aligned} a_h^E(v_h, v_h) &= \sum_{\widehat{E}\in E} \widehat{a}_h^E(\Pi^\dagger(v_h), \Pi^\dagger(v_h)) \simeq \sum_{\widehat{E}\in E} \|\Pi^\dagger(v_h)\|^2_{1,\widehat{h},\widehat{E}} \\ &= \|\Pi^\dagger(v_h)\|^2_{1,\widehat{h},E} \simeq \|v_h\|^2_{1,h,E}. \end{aligned}$$

We now observe that, for all linear functions $q$ in $\Omega$ and for every $E \in \Omega_h$ it holds

$$\begin{aligned} q(\mathsf{m}) &= \frac{1}{2}\big(q(\mathsf{v}_\mathsf{m}) + q(\mathsf{v}'_\mathsf{m})\big) \quad \forall \mathsf{m} = \mathsf{m}(e),\ e \in \partial E \\ q(\mathbf{x}_E) &= \frac{1}{N}\sum_{\mathsf{v}\in\partial E} q(\mathsf{v}). \end{aligned}$$

Therefore, it is immediate to check that the interpolant $q_I$ into the coarse space satisfies

$$\Pi^\dagger(q_I) = q_{\widehat{I}}, \tag{26}$$

where the symbol $\widehat{I}$ denotes the interpolation operator into the fine space $\widehat{V}_h$, analogous to (3). Therefore, using (25), (26) and ($\widehat{\mathsf{S}}$2) we get

$$\begin{aligned} a_h^E(v_h, q^I) &= \sum_{\widehat{E}\in E} \widehat{a}_h^{\widehat{E}}(\Pi^\dagger(v_h), \Pi^\dagger(q_I)) = \sum_{\widehat{E}\in E} \widehat{a}_h^{\widehat{E}}(\Pi^\dagger(v_h), q_{\widehat{I}}) \\ &= \sum_{\widehat{E}\in E} \sum_{\widehat{e}\in\partial\widehat{E}} (\nabla q \cdot \mathbf{n}_{\widehat{E}}^{\widehat{e}}) \frac{|\widehat{e}|}{2} \Big[ \big(\Pi^\dagger(v_h)\big)(\widehat{\mathsf{v}}_1) + \big(\Pi^\dagger(v_h)\big)(\widehat{\mathsf{v}}_2) \Big] \end{aligned} \tag{27}$$

where $\widehat{\mathsf{v}}_1$, $\widehat{\mathsf{v}}_2$ indicate the two vertexes of the fine edge $\widehat{e} \in \partial\widehat{E}$. The proof of ($\mathsf{S}2$) follows from using (27) and definition (15), and observing that the contribution of the fine edges that are internal to $E$ vanishes since all considered functions are single valued on such edges. □

Similarly, we can also define a loading term

$$(f, v_h)_h = \sum_{E\in\Omega_h} \sum_{\widehat{E}\in E} (f, \Pi^\dagger(v_h))_{\widehat{h},\widehat{E}}$$

where $(f,\cdot)_{\widehat{h},\widehat{E}}$ represents a local loading operator on the fine mesh following a construction analogous to (10).

Building the global bilinear form $a_h(\cdot,\cdot)$ that follows by summation of the local forms (25), and considering the load term above, we can define a discrete mimetic problem (11) on the coarse space. Such coarse problem has the advantage of being fully consistent with the fine problem. The usefulness of this construction will be clear in the next section.

### 4.3 A posteriori error analysis

We introduce the following fluctuation discrete problem:

$$\begin{cases} \text{Find } \widehat{e}_h^f \in \widehat{V}_h^f \text{ such that} \\ \widehat{a}_h(\widehat{e}_h^f, v_h^f) = (f, v_h^f)_{\widehat{h}} - \widehat{a}_h(\Pi^\dagger u_h, v_h^f) \qquad \forall v_h^f \in \widehat{V}_h^f \ . \end{cases} \tag{28}$$

Note that the right-hand side in (28) is the residual of the approximate solution $u_h$ when tested with the fluctuation space $\widehat{V}_h^f$.

In the sequel, we will work under the following *saturation assumption*:

($\mathsf{H}4$) There exists $\beta < 1$ such that

$$\|u_{\widehat{I}} - \widehat{u}_h\|_{1,\widehat{h}} \le \beta \ \|u_{\widehat{I}} - \Pi^\dagger u_h\|_{1,\widehat{h}} \ . \tag{29}$$

Assumption ($\mathsf{H}4$) simply means that the enriched discrete solution $\widehat{u}_h$ converges more rapidly than $u_h$ to the interpolant of the exact solution $u_{\widehat{I}}$. The validity of the saturation assumption is widely accepted in a posteriori error analysis of finite element methods [1, 5, 12], while its connection with small data oscillation has been explored in [20].

**Theorem 4.1 (upper bound)** *Assume (H1)-(H4). Let $u$ solve (1), let $u_h$ solve (11) and let $\widehat{e}_h^f$ solve (28). Let $c^* = \frac{1}{C_m(1-\beta)\widehat{c}_1}$, with $C_m$ as in (16). Then it holds:*

$$\|u_{\widehat{I}} - \Pi^\dagger u_h\|_{1,\widehat{h}} \leq c^* \Big( \widehat{c}_2 \|\widehat{e}_h^f\|_{1,\widehat{h}} + \sup_{v_h \in V_h} \frac{(f, \Pi^\dagger v_h)_{\widehat{h}} - \widehat{a}_h(\Pi^\dagger u_h, \Pi^\dagger v_h)}{\|\Pi^\dagger v_h\|_{1,\widehat{h}}} \Big) . \tag{30}$$

*Proof.* The triangle inequality and the saturation assumption (29) imply

$$(1-\beta)\|u_{\widehat{I}} - \Pi^\dagger u_h\|_{1,\widehat{h}} \leq \|\widehat{u}_h - \Pi^\dagger u_h\|_{1,\widehat{h}} \leq (1+\beta)\|u_{\widehat{I}} - \Pi^\dagger u_h\|_{1,\widehat{h}} \tag{31}$$

Let us prove (30). By using ($\widehat{\mathsf{S}}$1), (13), (28) and (16) we obtain

$$\begin{aligned}
\widehat{c}_1\|\widehat{u}_h - \Pi^\dagger u_h\|_{1,\widehat{h}} \ &\leq \sup_{\Pi^\dagger v_h + v_h^f \in \widehat{V}_h} \frac{\widehat{a}_h(\widehat{u}_h - \Pi^\dagger u_h, \Pi^\dagger v_h + v_h^f)}{\|\Pi^\dagger v_h + v_h^f\|_{1,\widehat{h}}} \\
&= \sup_{\Pi^\dagger v_h + v_h^f \in \widehat{V}_h} \frac{\widehat{a}_h(\widehat{u}_h, \Pi^\dagger v_h + v_h^f) - \widehat{a}_h(\Pi^\dagger u_h, \Pi^\dagger v_h + v_h^f)}{\|\Pi^\dagger v_h + v_h^f\|_{1,\widehat{h}}} \\
&= \sup_{\Pi^\dagger v_h + v_h^f \in \widehat{V}_h} \frac{(f, \Pi^\dagger v_h + v_h^f)_{\widehat{h}} - \widehat{a}_h(\Pi^\dagger u_h, \Pi^\dagger v_h) - (f, v_h^f)_{\widehat{h}} + (f, v_h^f)_{\widehat{h}} - \widehat{a}_h(\Pi^\dagger u_h, v_h^f)}{\|\Pi^\dagger v_h + v_h^f\|_{1,\widehat{h}}} \\
&= \sup_{\Pi^\dagger v_h + v_h^f \in \widehat{V}_h} \frac{(f, \Pi^\dagger v_h)_{\widehat{h}} + (f, v_h^f)_{\widehat{h}} - \widehat{a}_h(\Pi^\dagger u_h, \Pi^\dagger v_h) - (f, v_h^f)_{\widehat{h}} + \widehat{a}_h(e_h^f, v_h^f)}{\|\Pi^\dagger v_h + v_h^f\|_{1,\widehat{h}}} \\
&= \sup_{\Pi^\dagger v_h + v_h^f \in \widehat{V}_h} \frac{\widehat{a}_h(e_h^f, v_h^f) + (f, \Pi^\dagger v_h)_{\widehat{h}} - \widehat{a}_h(\Pi^\dagger u_h, \Pi^\dagger v_h)}{\|\Pi^\dagger v_h + v_h^f\|_{1,\widehat{h}}} \\
&\leq \frac{1}{C_m} \Big( \widehat{c}_2 \|e_h^f\|_{1,\widehat{h}} + \sup_{v_h \in V_h} \frac{(f, \Pi^\dagger v_h)_{\widehat{h}} - \widehat{a}_h(\Pi^\dagger u_h, \Pi^\dagger v_h)}{\|\Pi^\dagger v_h\|_{1,\widehat{h}}} \Big) .
\end{aligned}$$

Finally estimate (30) results from (31). □

The above result is general with respect to the choice of the bilinear forms $a_h$ and $\widehat{a}_h$. Nevertheless, the following particular case is relevant.

**Corollary 4.1 (upper bound)** *Assume (H1)-(H4) and that the coarse biliner form $a_h(\cdot,\cdot)$ is chosen according to (25). Let $u$ solve (1), let $u_h$ solve (11) and let $\widehat{e}_h^f$ solve (28). Let $c^* = \frac{1}{C_m(1-\beta)\widehat{c}_1}$, with $C_m$ as in (16). Then, it holds:*

$$\|u_{\widehat{I}} - \Pi^\dagger u_h\|_{1,\widehat{h}} \leq c^* \widehat{c}_2 \|\widehat{e}_h^f\|_{1,\widehat{h}} . \tag{32}$$

*Proof.* The proof immediately follows observing that

$$\widehat{a}_h(\Pi^\dagger u_h, \Pi^\dagger v_h) = (f, \Pi^\dagger v_h)_{\widehat{h}} \quad \forall v_h \in V_h ,$$

and thus the upper bound (30) reduces to the one shown above. □

**Remark 4.2** *We remark that it holds:*

$$\Pi(u_{\widehat{I}} - \Pi^\dagger u_h) = u_I - u_h.$$

*Therefore, using* (23)*, the left-hand sides of the upper bounds* (30) *and* (32) *may be replaced by the slightly more natural error quantity*

$$\|u_I - u_h\|_{1,h}.$$

**Theorem 4.2 (lower bound)** *Assume (H1)-(H4). Let $u$ solve* (1)*, let $u_h$ solve* (11) *and let $\widehat{e}_h^f$ solve* (28)*. If $c_* = \frac{\widehat{c}_2(1+\beta)}{\widehat{c}_1^f}$, then*

$$\|e_h^f\|_{1,\widehat{h}} \leq c_* \|u_{\widehat{I}} - \Pi^\dagger u_h\|_{1,\widehat{h}} \ . \tag{33}$$

*Proof.* Let us prove (33). We start noting that, from the stability condition ($\widehat{\mathsf{S1}}$), it follows

$$\widehat{c}_1^f \|v_h^f\|_{1,\widehat{h}}^2 \leq \widehat{a}_h(v_h^f, v_h^f) \quad \forall v_h^f \in \widehat{V}_h^f \ , \tag{34}$$

with $\widehat{c}_1^f$ a positive constant independent of $h$.

Thus, by using the above bound, the assumption ($\widehat{\mathsf{S1}}$), equations (28) and (13) we obtain

$$\begin{aligned}
\widehat{c}_1^f \|e_h^f\|_{1,\widehat{h}} &\leq \sup_{v_h^f \in V_h^f} \frac{\widehat{a}_h(e_h^f, v_h^f)}{\|v_h^f\|_{1,\widehat{h}}} \\
&= \sup_{v_h^f \in V_h^f} \frac{(f, v_h^f)_{\widehat{h}} - \widehat{a}_h(\Pi^\dagger u_h, v_h^f)}{\|v_h^f\|_{1,\widehat{h}}} \\
&= \sup_{v_h^f \in V_h^f} \frac{\widehat{a}_h(\widehat{u}_h, v_h^f) - \widehat{a}_h(\widehat{u}_h, v_h^f) + (f, v_h^f)_{\widehat{h}} - \widehat{a}_h(\Pi^\dagger u_h, v_h^f)}{\|v_h^f\|_{1,\widehat{h}}} \\
&= \sup_{v_h^f \in V_h^f} \frac{(f, v_h^f)_{\widehat{h}} - \widehat{a}_h(\widehat{u}_h, v_h^f) + \widehat{a}_h(\widehat{u}_h - \Pi^\dagger u_h, v_h^f)}{\|v_h^f\|_{1,\widehat{h}}} \\
&\leq \widehat{c}_2 \|\widehat{u}_h - \Pi^\dagger u_h\|_{1,\widehat{h}} + \sup_{v_h^f \in V_h^f} \frac{(f, v_h^f)_{\widehat{h}} - \widehat{a}_h(\widehat{u}_h, v_h^f)}{\|v_h^f\|_{1,\widehat{h}}} \\
&= \widehat{c}_2 \|\widehat{u}_h - \Pi^\dagger u_h\|_{1,\widehat{h}} \ .
\end{aligned} \tag{35}$$

Estimate (33) then results from (31). □

**Remark 4.3** *If* (28) *is replaced by a more general fluctuation problem*

$$\widehat{b}_h(\widehat{e}_h^f, v_h^f) = ((f, v_h^f))_{\widehat{h}} - \widehat{a}_h(\Pi^\dagger u_h, v_h^f) \qquad \forall v_h^f \in \widehat{V}_h^f \ , \tag{36}$$

*with suitable $\widehat{b}_h(\cdot,\cdot)$ satisfying (($\widehat{\mathsf{S1}}$)-($\widehat{\mathsf{S2}}$)) and $((\cdot,\cdot))_{\widehat{h}}$, then the upper bound* (30) *and the lower bound* (33) *still hold (with different constants), provided the following new consistency term is added on the corresponding right-hand sides*

$$\sup_{v_h^f \in \widehat{V}_h^f} \frac{(f, v_h^f)_{\widehat{h}} - ((f, v_h^f))_{\widehat{h}}}{\|v_h^f\|_{1,\widehat{h}}} \ . \tag{37}$$

**Remark 4.4 (local error indicators)** *The upper bound* (32) *can be rewritten in the following way*

$$\|u_{\widehat{I}} - \Pi^\dagger u_h\|^2_{1,\widehat{h}} \leq \left(c^* \widehat{c}_2\right)^2 \sum_{E \in \Omega_h} \eta_E^2$$

*with* $\eta_E^2 := \sum_{\widehat{E} \in E} \|e_h^f\|^2_{1,\widehat{h},\widehat{E}}$. *The quantities* $\eta_E$ *will be employed as local error indicators in the marking step of the adaptive algorithm implemented in Section 5.*

**Remark 4.5 (inexpensive heuristic error indicators)** *The computation of the error indicator* $\eta_E$ *is quite demanding as it requires the solution of the discrete problem* (28)*, whose cost is comparable to that of solving the original problem. With the aim of reducing the computational burden, we follow the ideas of [4] and we introduce inexpensive heuristic error indicators. This is obtained following the same steps as in the derivation of* $\eta_E$*, but substituting the stiffness matrix in system* (28) *with its diagonal part. This procedure turns out to be computationally advantageous as it is equivalent to solving uncoupled local problems with (edge and element) bubble type functions. The ensuing local heuristic error indicator is labeled as* $\eta_E^D := \sum_{\widehat{E} \in E} \|\overline{e}_h^f\|^2_{1,\widehat{h},\widehat{E}}$ *being* $\overline{e}_h^f$ *the solution of problem* (28) *where only the diagonal part of the stiffness matrix is employed. Note that all the previous theoretical results are lost; nevertheless, the numerical tests in Section 5 will show the efficacy of the new heuristic error indicators in driving adaptive algorithms.*

# 5 Numerical experiments

In this section we present a series of numerical examples to illustrate the performance of the proposed a posteriori error indicators combined with an automatic adaptive refinement procedure.

## 5.1 The estimator $\eta$

This subsection concerns with the estimator $\eta$ defined by $\eta^2 := \sum_{E \in \Omega_h} \eta_E^2$, where $\eta_E$ are given in Remark 4.4. We test its numerical performance on a couple of significant examples.

We also recall that, in order to measure the quality of the computed bounds, we define the a posteriori *effectivity index* as the ratio of the a posteriori error estimator $\eta$ and the energy norm of the error $\|u - \Pi^\dagger u_h\|_{1,\widehat{h}}$, when the analytical solution is available.

### 5.1.1 Example 1

We let $\Omega = (0,1)^2$ and select $f$ so that the analytical solution to (1) is given by

$$u(x,y) = \frac{1 - \exp(-100x)}{1 - \exp(-100)} \sin(\pi y)(1-x).$$

As shown in Figure 2, the analytical solution exhibits a strong boundary layer along the line $x = 0$.

We first investigate the performance of the proposed error estimator $\eta$ using the set of initial uniform meshes depicted in Figure 3 (top), and considering $n = 1, 2, 3, 4$ successive uniform refinements of the initial grids. To refine elements we employed the strategy described

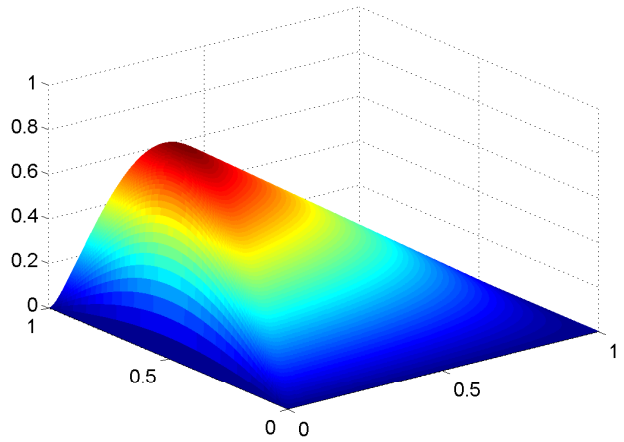


Figure 2: Example 2. Analytical solution.

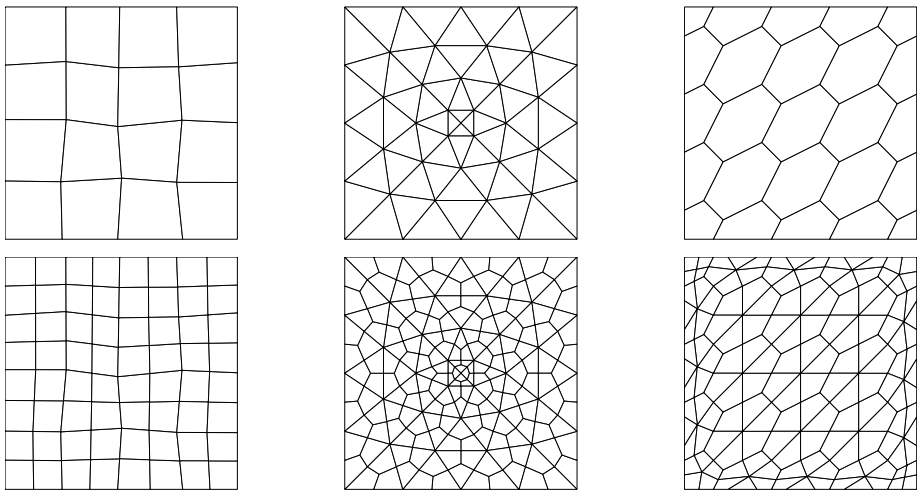

Figure 3: Top: initial quadrilateral (Test A), triangular (Test B), and hexagonal (Test C) grids. Bottom: first level of uniformly refined grids.

in Section 4.1 (cf. Figure 3 (bottom) for the first level of uniformly refined grids). In Figure 4 (loglog-scale) we present a comparison of the actual and estimated discrete energy norm of the error versus the number of degrees of freedom, on the sequence of uniformly refined meshes. For the sake of comparison, Figure 4 also show the discrete energy error computed on the current mesh, namely $\|u - u_h\|_{1,h}$.

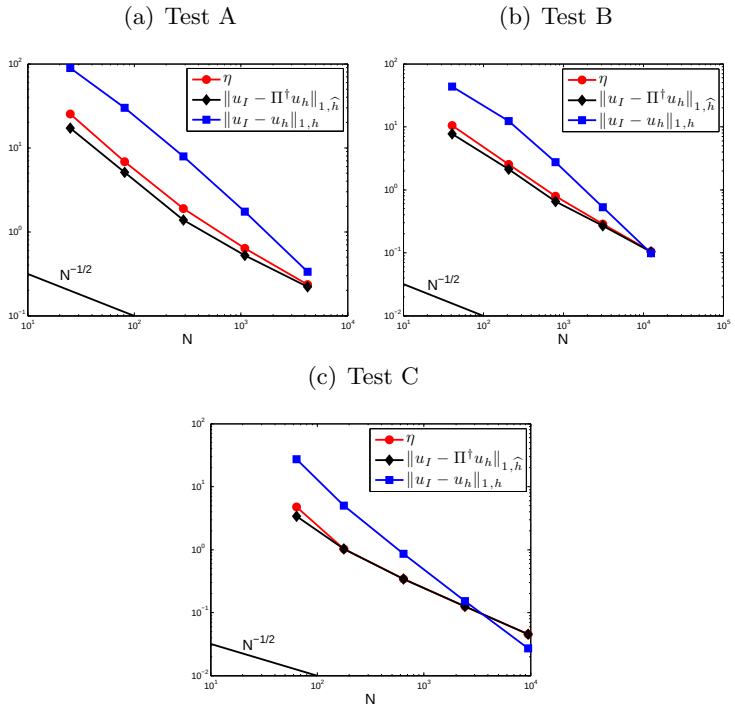


Figure 4: Example 1. Actual and estimated errors versus the number of degrees of freedom (uniformly refined grids). Loglog-scale.

As predicted by our theoretical results, the actual error $\|u - \Pi^\dagger u_h\|_{1,\widehat{h}}$ and the a posteriori error estimator $\eta$ go to zero as $h$ goes to zero at the same rate. We also observe that the discrete energy error computed on the current mesh $\|u - u_h\|_{1,h}$ goes to zero with a moderately better rate than expected; such a behavior has been already observed in previous papers.

Next we investigate the performance of the proposed error estimator combined with an $h$-adaptive refinement procedure of the form:

$$\texttt{SOLVE} \rightarrow \texttt{ESTIMATE} \rightarrow \texttt{MARK} \rightarrow \texttt{REFINE}.$$

Here `SOLVE` computes the discrete solution. The module `ESTIMATE` makes use of the upper bound (30) (see also Remark 4.4) to calculate the error indicators, while the procedure `MARK` employs the fixed fraction strategy, with refinement fraction set to 30%, to make a selection of the elements to be refined. Finally, the module `REFINE` uses the strategy described in Section 4.1 to subdivide elements marked for refinement.

We test the performance of the proposed a posteriori error estimator on a set of different initial uniform grids as the ones reported in Figure 3 (top).

Figure 5 shows, for all the considered initial grids, the computational meshes obtained after two (top), four (middle), and six (bottom) adaptive refinement steps, respectively.

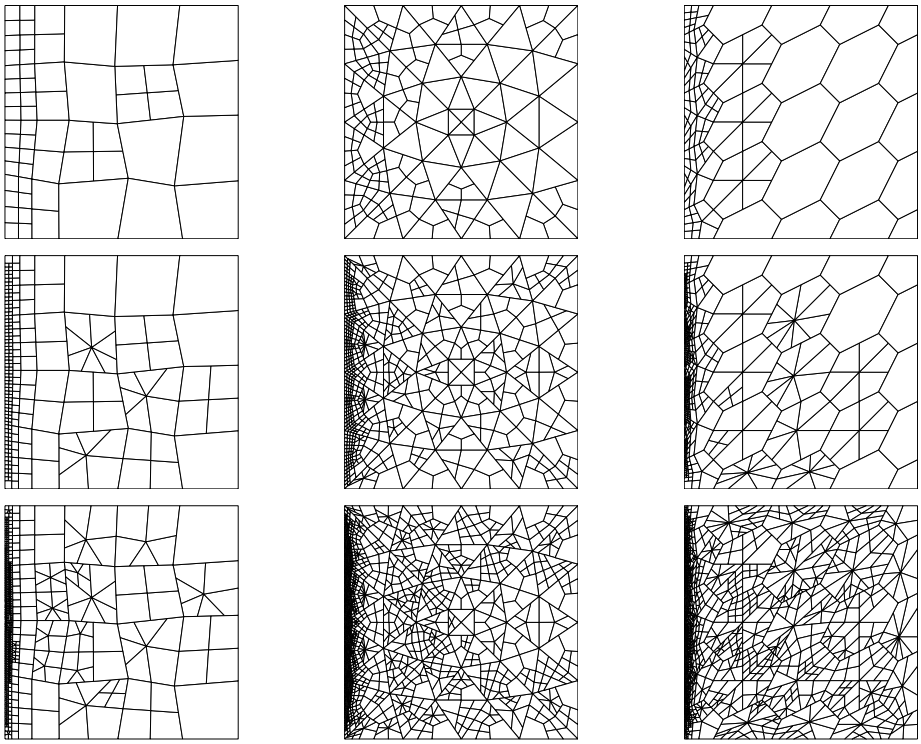

Figure 5: Example 1. Computational meshes after two (top), four (middle), and six (bottom) adaptive refinements.

Figure 6 (left) reports the computed effectivity indexes for all the grid configurations considered. As expected, on all the mesh configurations considered, the effectivity index is roughly constant on the sequence of non-uniform meshes generated by the adaptive refinement algorithm.

Furthermore, we compare the accuracy of the approximation of the computed solutions on the sequence of adaptively and uniformly refined grids. Figure 6 (right) shows for all the mesh configurations considered a comparison between the actual errors $\|u - \Pi^{\dagger} u_h\|_{1,\widehat{h}}$ computed on the sequence of meshes generated by the uniform and the adaptive refinement strategy. We clearly observe that, as expected, adaptive strategy overperform the non-adaptive one.

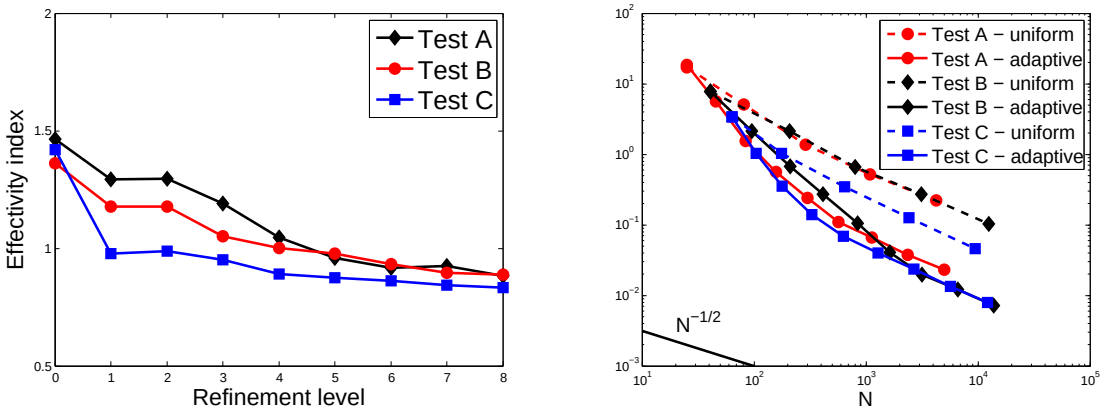


Figure 6: Example 1. Left: effectivity indexes on the sequence of non-uniform meshes. Right: comparison between the actual errors $\|u - \Pi^{\dagger} u_h\|_{1,\widehat{h}}$ computed on the sequence of uniformly refined and adapted grids (loglog-scale).

Finally, Figure 7 shows a plot of the fluctuation error $\widehat{e}_h^f$ on the initial mesh configuration of Test C and on the corresponding mesh generated after two steps of the adaptive refinement strategy.

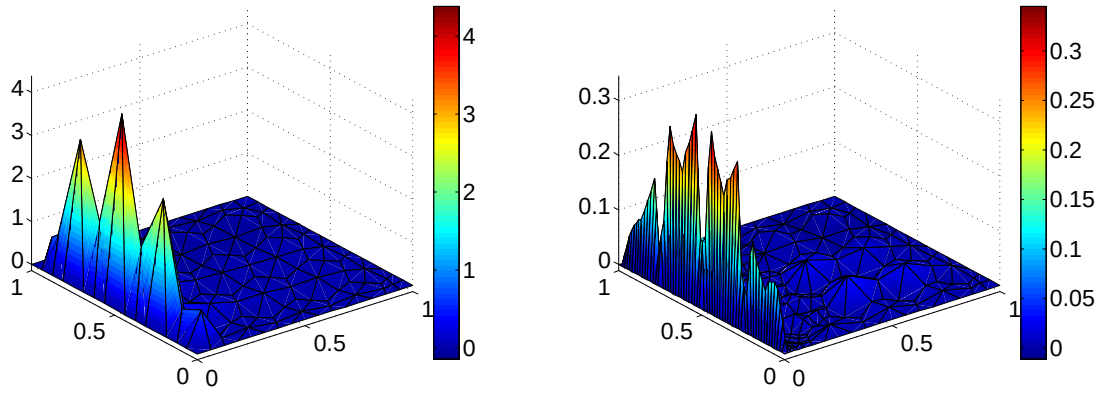

Figure 7: Example 1. Fluctuation error $\widehat{e}_h^f$ on the initial mesh configuration of Test C (left) and on the adaptive mesh constructed after two steps of refinement by employing the fixed fraction marking strategy (right).

### 5.1.2 Example 2

We consider the model problem on a L-shaped domain $\Omega$, obtained carving out the lower right quarter from the square domain $(-1, 1)^2$. We select $f = 0$ and, writing $(\rho, \theta)$ to denote the system of polar coordinates, we impose an appropriate inhomogeneous boundary condition for the exact solution $u$ so that

$$u(\rho, \theta) = \rho^{2/3} \sin(2\theta/3).$$

We emphasize that $u$ is analytic in $\overline{\Omega} \setminus \{0\}$, but $\nabla u$ is singular at the origin; indeed, here $u \notin H^2(\Omega)$

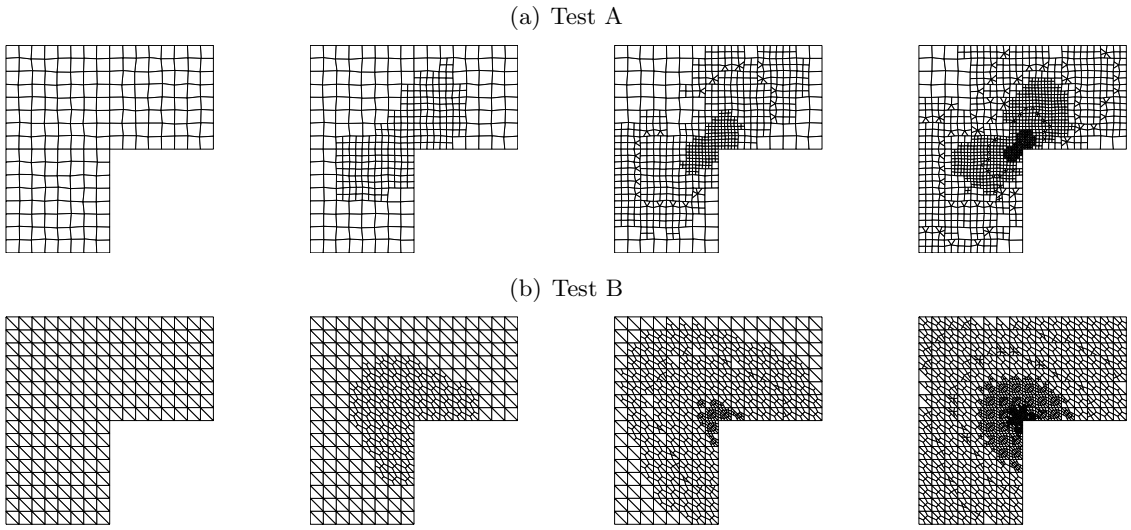


Figure 8: Example 2. Initial mesh configurations of Test A (top) and Test B (bottom), and the first three levels of computational meshes generated by the adaptive refinement strategy employing the fixed fraction marking strategy.

In Figure 8 we report the initial mesh configurations considered together with the first three levels of meshes generated by the adaptive algorithm employing the fixed fraction marking strategy. We clearly observe that the mesh is refined near the singularity. In Figure 9 the error estimator computed on the sequence of the adaptively generated meshes together with the actual error in the discrete energy norm are plotted as a function of the number of degrees of freedom (loglog-scale). Figure 10 shows a plot of the fluctuation error $\widehat{e}_h^f$ on the initial

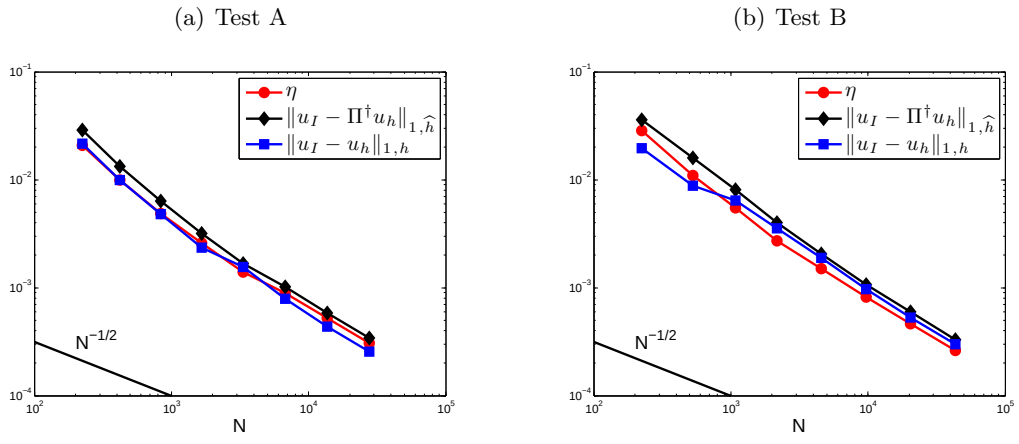


Figure 9: Example 2. Actual and estimated errors versus the number of degrees of freedom (loglog-scale). The adaptive meshes are constructed by employing the fixed fraction marking strategy.

mesh configuration of Test B and on the corresponding mesh generated after three steps of the adaptive refinement strategy. We can observe, as expected, that the error is concentrated near the origin where the gradient of the exact solution exhibits a singularity.

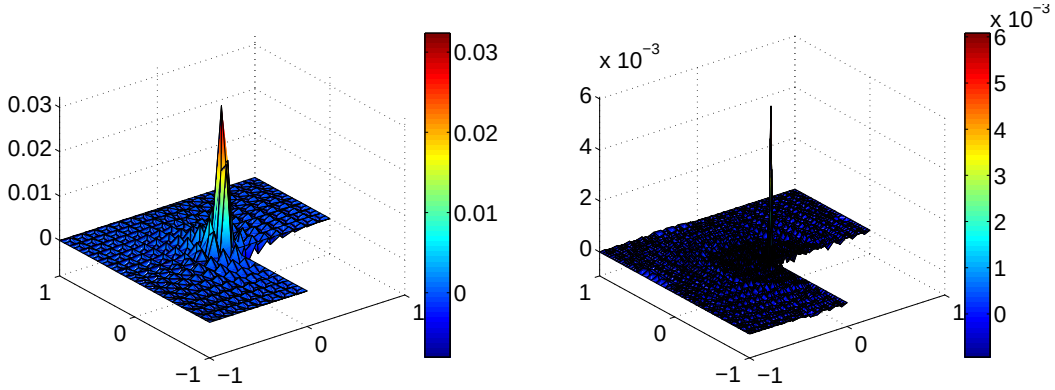


Figure 10: Example 2. Fluctuation error $\widehat{e}_h^f$ on the initial mesh configuration of Test B (left) and on the adaptive meshes constructed after three steps of refinement by employing the fixed fraction marking strategy (right).

Next, we address the performance of our *a-posteriori* error estimator combined with a different marking strategy. To this aim, we consider the Dörfler marking strategy [19], which we briefly recall in the following. Sort the local error indicators $\{\eta_E\}_{E\in\Omega_h}$ such that $\eta_{E_{k-1}} \geq \eta_{E_k}$ for $k = 2, \ldots, \#\Omega_h$. The set of elements marked for refinement is given by $\{\eta_{E_k}\}_{k=1,\ldots,s}$, where $s$ is the smallest integer such that

$$\sum_{k=1}^{s} \eta_{E_k} \geq \theta \sum_{k=1}^{\#\Omega_h} \eta_{E_k}, \quad \theta \in [0,1).$$

We have run the same set of numerical experiments as before starting again from the initial mesh configurations shown in Figure 8 (left): the first three levels of meshes generated by the adaptive algorithm are shown in Figure 11. Figure 12 (loglog-scale) shows the error estimator computed on the corresponding sequence of adaptively generated grids together with the actual error in the discrete energy norm as a function of the number of degrees of freedom. We clearly observe that by employing the Dörfler marking strategy the mesh refinement is much more concentrated near the region where the exact solution exhibits a singularity, at least in the first refinement levels. To compare the performance of the marking strategies, Figure 13 shows the the estimated errors computed on the sequence of adaptively refined meshes according to the different marking strategies. We can observe the marking strategies are asymptotically equivalent.

Finally, in Figure 14 we report the effectivity indexes computed on the sequence of meshes adaptively generated by the two marking strategies. As expected, the effectivity index is roughly constant on both the sequence of non-uniform meshes generated by the adaptive refinement algorithm.

(a) Test A

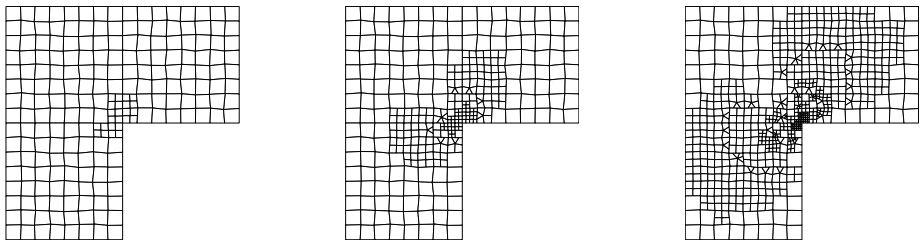

(b) Test B

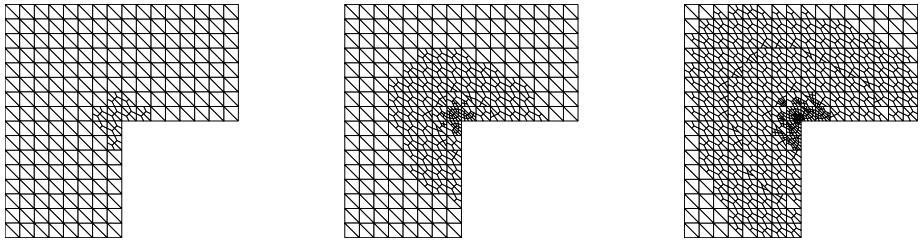

Figure 11: Example 2. First three levels of computational meshes generated by the adaptive refinement strategy for two different initial mesh configurations. The adaptive meshes are constructed by employing the Dörfler marking strategy.

(a) Test A

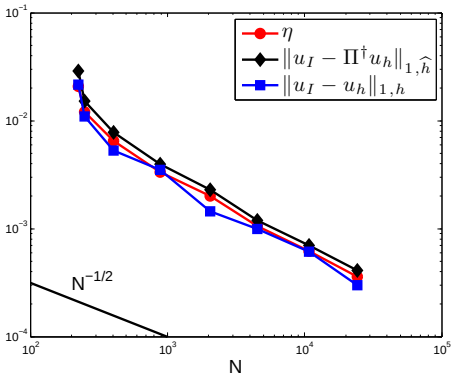


(b) Test B

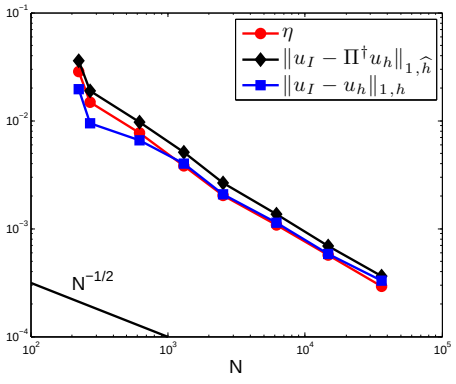


Figure 12: Example 2. Actual and estimated errors versus the number of degrees of freedom (loglog-scale). The adaptive meshes are constructed by employing the Dörfler marking strategy.

(a) Test A (b) Test B

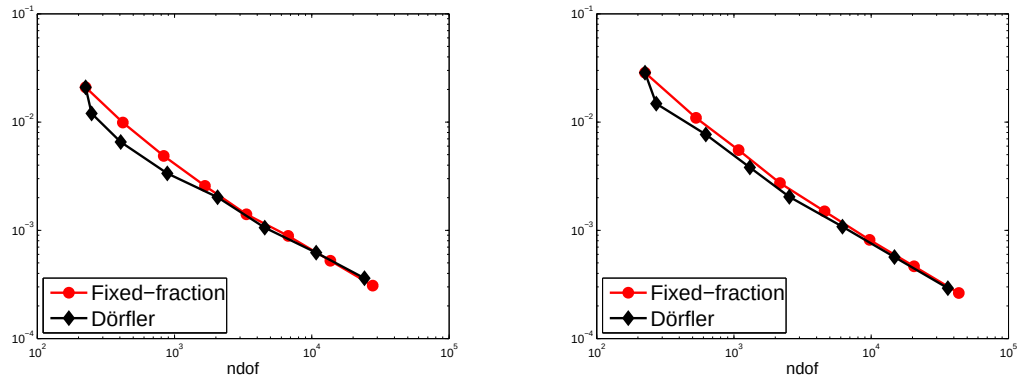


Figure 13: Example 2. Estimated errors versus the number of degrees of freedom for adaptively refined meshes (loglog-scale) according to different marking strategies.

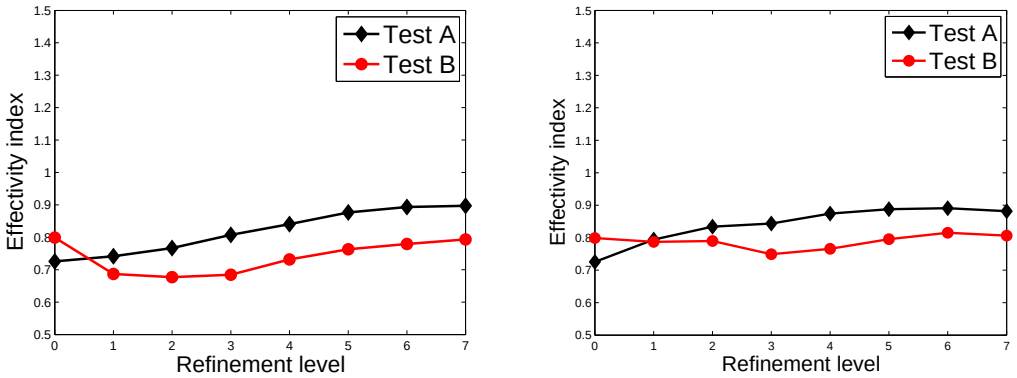


Figure 14: Example 2. Effectivity indeces on the sequence of the adaptive meshes constructed by employing the fixed fraction strategy (left) and the Dörfler strategy (right).

## 5.2 The heuristic estimator $\eta^D$

In this last subsection we show the results obtained with the inexpensive heuristic error indicators proposed in Remark 4.5. We denote by $\eta^D$ the counterpart of $\eta$ when the local error indicators $\eta_E^D$ are employed. In the following we consider the same test problems as in Sections 5.1.1 and 5.1.2 where in all cases the fixed fraction strategy is adopted.

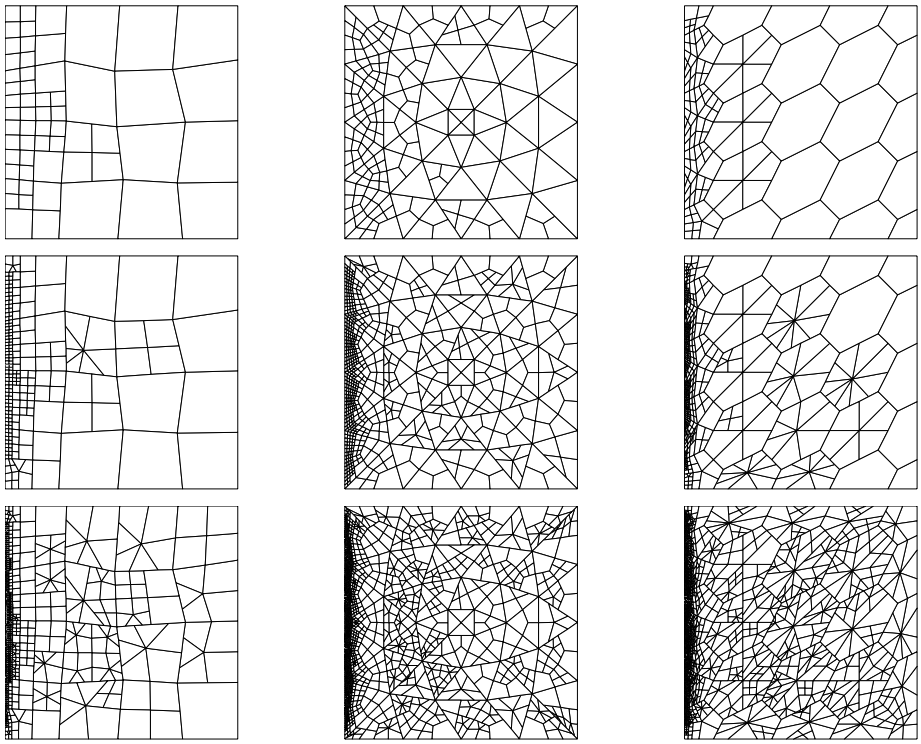

Figure 15: Example 1. Heuristic estimator $\eta^D$. Computational meshes after two (top), four (middle), and six (bottom) adaptive refinements (fixed-fraction strategy).

We first show the results for *Example 1* (see Section 5.1.1). In Figure 15 we depict some computational meshes obtained with the adaptive strategy driven by the error indicators $\eta_E^D$. Such meshes are correctly refined towards the left hand side boundary. In Figure 16 we show a comparison between the discrete norm errors and the total error estimator $\eta^D$.

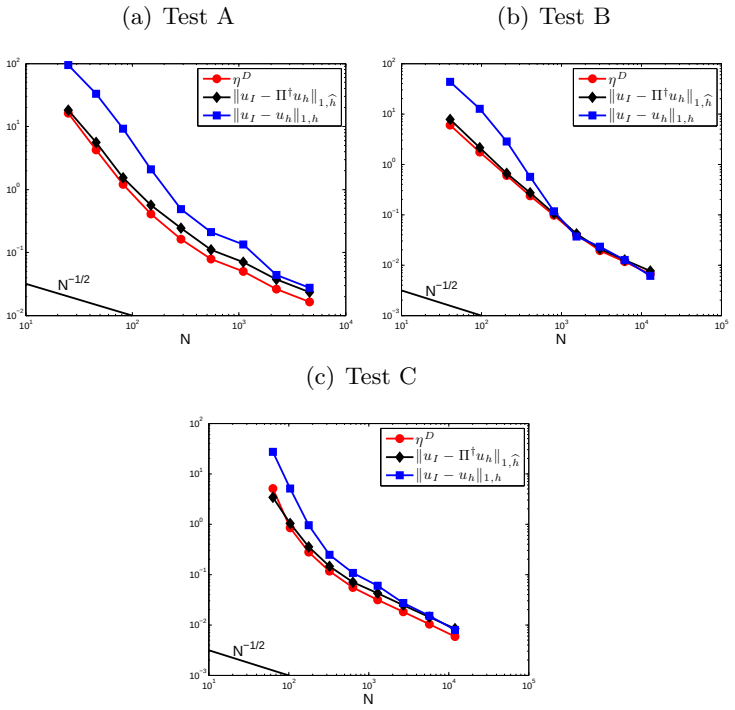


Figure 16: Example 1. Heuristic estimator $\eta^D$. Actual and estimated errors versus the number of degrees of freedom (adaptively refined grids, fixed-fraction startegy). Loglog-scale.

The analogous results for *Example 2* (see Section 5.1.2) are shown in Figures 17-18. In particular, note that the meshes are correctly refined towards the re-entrant corner.

In Figure 19, the effectivity index behavior is plotted for both *Example 1* and *Example 2*: we can clearly observe that in both cases the effectivity index gets quite close to the optimal value of one.

We finally remark that all the outcomes for $\eta^D$, which are also to be compared with the corresponding ones for $\eta$ in Sections 5.1.1 and 5.1.2, suggest that the former estimator has a general satisfactory behaviour. Therefore, due its very convenient computational cost, the estimator $\eta^D$ may be preferable to $\eta$ in many cases of practical interest.

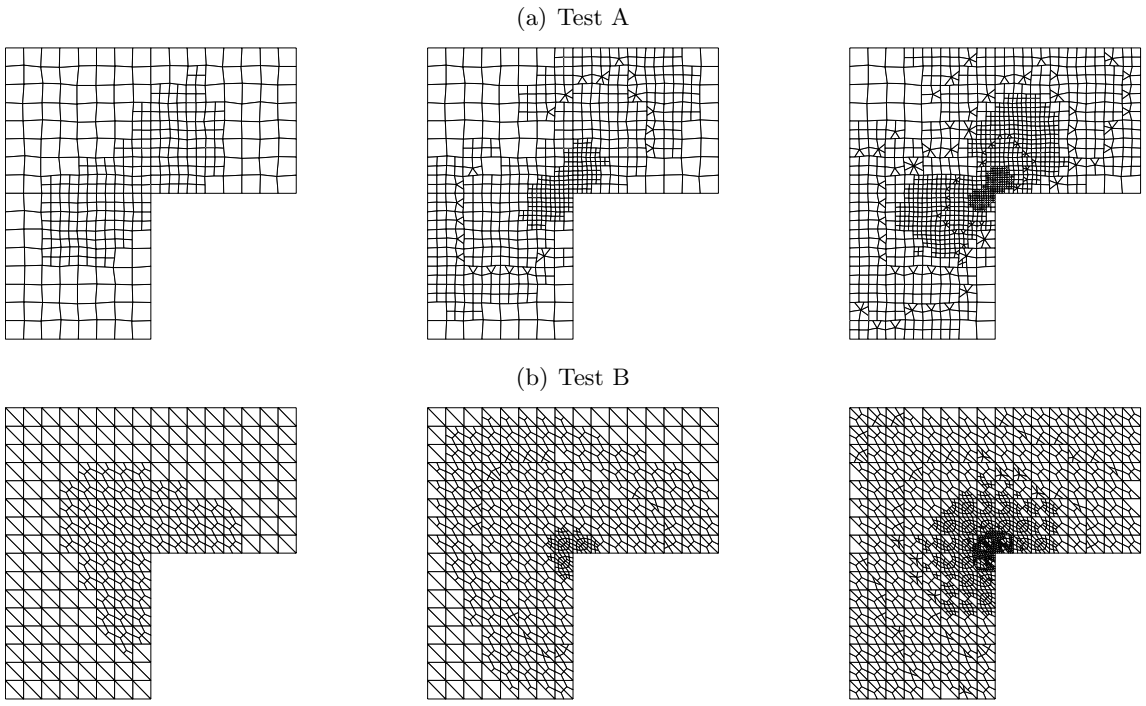


Figure 17: Example 2. Heuristic estimator $\eta^D$. First three levels of computational meshes generated by the adaptive refinement strategy for two different initial mesh configurations. The adaptive meshes are constructed by employing the fixed-fraction strategy.

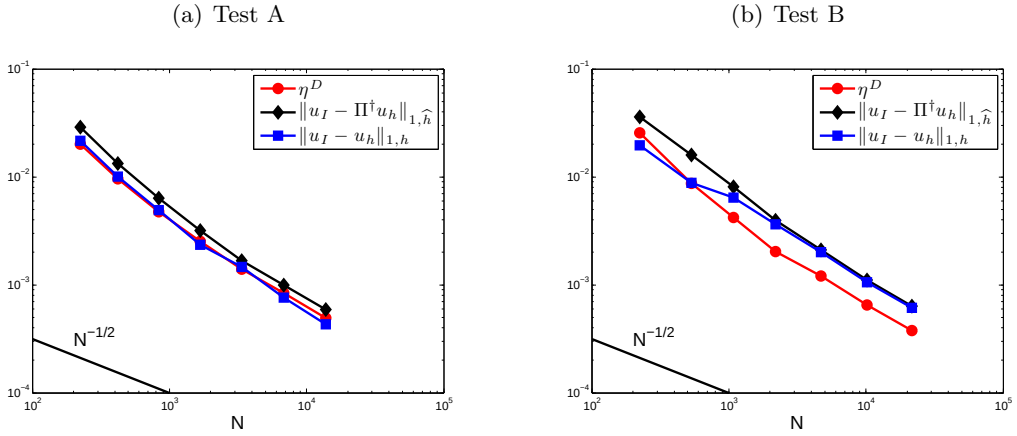


Figure 18: Example 2. Heuristic estimator $\eta^D$. Actual and estimated errors versus the number of degrees of freedom (adaptively refined grids, fixed-fraction startegy). Loglog-scale.

(a) Example 1 (b) Example 2

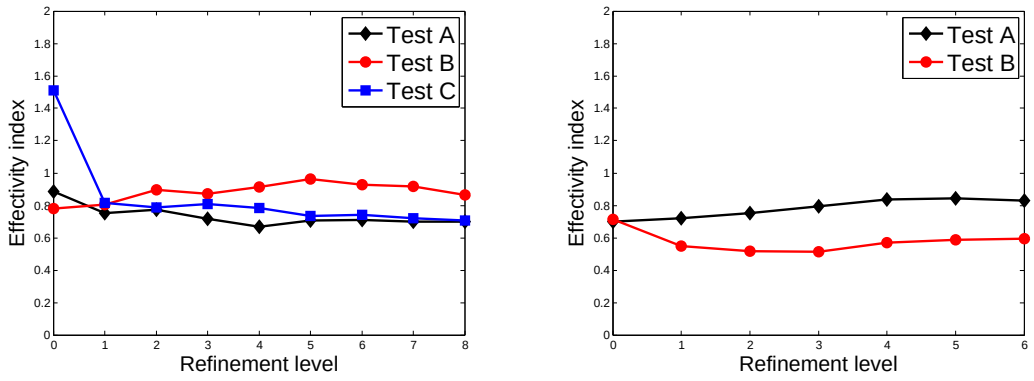


Figure 19: Heuristic estimator $\eta^D$. Effectivity indexes on the sequence of adaptively refined meshes. The sequence of adaptive meshes is constructed by employing the fixed fraction strategy.

## References


[1] Mark Ainsworth and J. Tinsley Oden. *A posteriori error estimation in finite element analysis*. Pure and Applied Mathematics (New York). Wiley-Interscience [John Wiley & Sons], New York, 2000.

[2] P.F. Antonietti, L. Beirão da Veiga, and M. Verani. A mimetic discretization of elliptic obstacle problems. Technical Report 14, MOX, Dipartimento di Matematica, Politecnico di Milano, Piazza Leonardo da Vinci, 32, 20133 Milano, Italy, 2010. http://mox.polimi.it/it/progetti/pubblicazioni/.

[3] Ivo Babuška and Theofanis Strouboulis. *The finite element method and its reliability*. Numerical Mathematics and Scientific Computation. The Clarendon Press Oxford University Press, New York, 2001.

[4] R. E. Bank. Hierarchical bases and the finite element method. *Acta Numerica*, 5:1–43, 1996.

[5] R. E. Bank and A. Weiser. Some a posteriori error estimators for elliptic partial differential equations. *Math. Comp.*, 44(170):283–301, 1985.

[6] L. Beirão da Veiga. A residual based error estimator for the mimetic finite difference method. *Numer. Math.*, 108(3):387–406, 2008.

[7] L. Beirão da Veiga. A mimetic finite difference method for linear elasticity. *Math. Model. Numer. Anal.*, 44:231–250, 2010.

[8] L. Beirão da Veiga, K. Lipnikov, and G. Manzini. Arbitrary order nodal mimetic discretizations of elliptic problems on polygonal meshes. In press on *SIAM J. Numer. Anal.*

[9] L. Beirão da Veiga, K. Lipnikov, and G. Manzini. Error analysis of a mimetic discretization for the steady Stokes problem on polyhedral meshes. *SIAM J. Numer. Anal.*, 48:1419–1443, 2010.

[10] L. Beirão da Veiga and G. Manzini. An a posteriori error estimator for the mimetic finite difference approximation of elliptic problems. *Int. J. Numer. Methods Engrg.*, 76(11):1696–1723, 2008.

[11] M. Berndt, K. Lipnikov, M. Shashkov, M. F. Wheeler, and I. Yotov. Superconvergence of the velocity in mimetic finite difference methods on quadrilaterals. *SIAM J. Numer. Anal.*, 43(4):1728–1749, 2005.

[12] Folkmar A. Bornemann, Bodo Erdmann, and Ralf Kornhuber. A posteriori error estimates for elliptic problems in two and three space dimensions. *SIAM J. Numer. Anal.*, 33(3):1188–1204, 1996.

[13] S. Brenner and L. Scott. *The Mathematical Theory of Finite Element Methods*. Springer-Verlag, Berlin/Heidelberg, 1994.

[14] F. Brezzi, A. Buffa, and K. Lipnikov. Mimetic finite differences for elliptic problems. *M2AN Math. Model. Numer. Anal.*, 43(2):277–295, 2009.

[15] F. Brezzi, K. Lipnikov, and M. Shashkov. Convergence of the mimetic finite difference method for diffusion problems on polyhedral meshes. *SIAM J. Numer. Anal.*, 43(5):1872–1896, 2005.

[16] F. Brezzi, K. Lipnikov, and M. Shashkov. Convergence of mimetic finite difference method for diffusion problems on polyhedral meshes with curved faces. *Math. Models Methods Appl. Sci.*, 16(2):275–297, 2006.

[17] A. Cangiani and G. Manzini. Flux reconstruction and pressure post-processing in mimetic finite difference methods. *Comput. Methods Appl. Mech. Engrg.*, 197(9-12):933–945, 2008.

[18] A. Cangiani, G. Manzini, and A. Russo. Convergence analysis of the mimetic finite difference method for elliptic problems. *SIAM J. Numer. Anal.*, 47(4):2612–2637, 2009.

[19] Willy Dörfler. A convergent adaptive algorithm for Poisson's equation. *SIAM J. Numer. Anal.*, 33(3):1106–1124, 1996.

[20] Willy Dörfler and Ricardo H. Nochetto. Small data oscillation implies the saturation assumption. *Numer. Math.*, 91(1):1–12, 2002.

[21] T. Dupont and R. Scott. Polynomial approximation of functions in Sobolev spaces. *Math. Comp.*, 34(150):441–463, 1980.

[22] J. Hyman, J. Morel, M. Shashkov, and S. Steinberg. Mimetic finite difference methods for diffusion equations. *Comput. Geosci.*, 6(3-4):333–352, 2002.

[23] J. Hyman, M. Shashkov, and S. Steinberg. The numerical solution of diffusion problems in strongly heterogeneous non-isotropic materials. *J. Comput. Phys.*, 132(1):130–148, 1997.

[24] K. Lipnikov, J. Morel, and M. Shashkov. Mimetic finite difference methods for diffusion equations on non-orthogonal non-conformal meshes. *J. Comput. Phys.*, 199(2):589–597, 2004.

[25] K. Lipnikov, M. Shashkov, and I. Yotov. Local flux mimetic finite difference methods. *Numer. Math.*, 112(1):115–152, 2009.

[26] J. Morel, R. Roberts, and M. Shashkov. A local support-operators diffusion discretization scheme for quadrilateral $r - z$ meshes. *J. Comput. Phys.*, 144(1):17–51, 1998.

[27] S. E. Mousavi, H. Xiao, and N. Sukumar. Generalized Gaussian quadrature rules on arbitrary polygons. *Internat. J. Numer. Methods Engrg.*, 82(1):99–113, 2010.

[28] Ricardo H. Nochetto, Kunibert G. Siebert, and Andreas Veeser. Theory of adaptive finite element methods: an introduction. In *Multiscale, nonlinear and adaptive approximation*, pages 409–542. Springer, Berlin, 2009.

[29] N. Sukumar and A. Tabarrei. Conformig polygonal finite elements. *Internat. J. Numer. Methods Engrg.*, 61:2045–2066, 2004.

[30] R. Verfürth. *A Review af A Posteriori Error Estimation and Adaptive Mesh-Refinement Technique*. Wiley-Teubner, 1996.

[31] Takaharu Yaguchi, Takayasu Matsuo, and Masaaki Sugihara. An extension of the discrete variational method to nonuniform grids. *J. Comput. Phys.*, 229(11):4382–4423, 2010.

# MOX Technical Reports, last issues

**Dipartimento di Matematica "F. Brioschi",**
**Politecnico di Milano, Via Bonardi 9 - 20133 Milano (Italy)**

**34/2011** Benacchio, T.; Bonaventura, L.
*A spectral collocation method for the one dimensional shallow water equations on semi-infinite domains*

**33/2011** Antonietti, P.F.; Beirao da Veiga, L.; Lovadina, C.; Verani, M.
*Hierarchical a posteriori error estimators for the mimetic discretization of elliptic problems*

**32/2011** Aletti, G; Ghiglietti, A; Paganoni, A.
*A modified randomly reinforced urn design*

**31/2011** Astorino, M.; Becerra Sagredo, J.; Quarteroni, A.
*A modular lattice Boltzmann solver for GPU computing processors*

**30/2011** Nobile, F.; Pozzoli, M.; Vergara, C.
*Time accurate partitioned algorithms for the solution of fluid-structure interaction problems in haemodynamics*

**29/2011** Morin, P.; Nochetto, R.H.; Pauletti, S.; Verani, M.
*AFEM for Shape Optimization*

**28/2011** Pischiutta, M.; Formaggia, L.; Nobile, F.
*Mathematical modelling for the evolution of aeolian dunes formed by a mixture of sands: entrainment-deposition formulation*

**27/2011** Antonietti, P.F.; Bigoni, N.; Verani, M.
*A Mimetic Discretization of Elliptic Control Problems*

**26/2011** Secchi, P.; Vantini, S.; Vitelli, V.
*Bagging Voronoi classifiers for clustering spatial functional data*

**25/2011** de Luca, M.; Ambrosi, D.; Robertson, A.M.; Veneziani, A.; Quarteroni, A.
*Finite element analysis for a multi-mechanism damage model of cerebral arterial tissue*